In Vivo Silicon-Based Flexible Radio Frequency Integrated Circuits Monolithically Encapsulated with Biocompatible Liquid Crystal Polymers

Geon-Tae Hwang,[†] Donggu Im,[‡] Sung Eun Lee,[§] Jooseok Lee,[‡] Min Koo,[†] So Young Park,[†] Seungjun Kim,[†] Kyounghoon Yang,[‡] Sung June Kim,[§] Kwyro Lee,[‡,⊥] and Keon Jae Lee[†,*]

[†]Department of Materials Science and Engineering and [‡]Department of Electrical Engineering, Korea Advanced Institute of Science and Technology (KAIST), 291 Daehak-ro, Yuseong-gu, Daejeon 305-701, Republic of Korea, [§]Department of Electrical Engineering and Computer Science, Seoul National University, 599 Gwanakno, Gwanak-gu, Seoul 151-744, Republic of Korea, and [⊥]National Nanofab Center, 291 Daehak-ro, Yuseong-gu, Daejeon 305-701, Republic of Korea

ABSTRACT Biointegrated electronics have been investigated for various healthcare applications which can introduce biomedical systems into the human body. Silicon-based semiconductors perform significant roles of nerve stimulation, signal analysis, and wireless communication in implantable electronics. However, the current large-scale integration (LSI) chips have limitations in *in vivo* devices due to their rigid and bulky properties. This paper describes *in vivo* ultrathin silicon-based liquid crystal polymer (LCP) monolithically encapsulated flexible radio frequency integrated circuits (RFICs) for medical wireless communication. The mechanical stability of the LCP encapsulation is supported by finite element analysis simulation. *In vivo* electrical reliability and bioaffinity of the LCP monoencapsulated RFIC devices are confirmed in rats. *In vitro* accelerated soak tests are performed with Arrhenius method to estimate the lifetime of LCP monoencapsulated RFICs in a live body. The work could provide an approach to flexible LSI in biointegrated electronics such as an artificial retina and wireless body sensor networks.

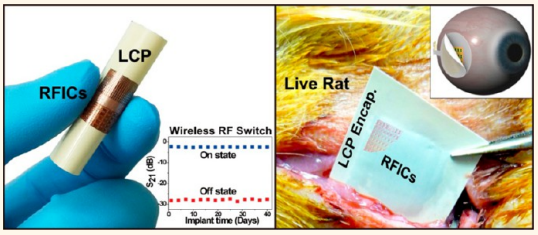

KEYWORDS: biointegrated electronics · flexible CMOS integrated circuits · silicon nanomembrane · biocompatible packaging · liquid crystal polymers · monolithic encapsulation

Biointegrated electronics have attracted great attention for realizing *in vivo* ubiquitous healthcare systems including wireless body sensor networks (BSNs), neural prosthetics, and remote treatment.[1−4] Since the implantable devices have to work even in a harsh environment like the hot, humid, and actively moving human body, their development has critical obstacles to overcome in terms of shapes and materials.[5] Many research teams have explored various types of flexible semiconductor materials such as organic thin films,[6] inorganic nanowires,[7] and graphitic carbons.[8,9] However, their insufficient carrier mobility, low drive current, and inaccurate positioning have restricted the range of applications as high-performance flexible electronics.[10]

Silicon-based large-scale integrated electronics for biomedical devices (*e.g.*, deep brain stimulator, cochlear implant) have played significant roles in neurological stimulation (*i.e.*, analog front end, AFE), signal processing, memory storage, and radio frequency (RF) wireless communication.[11−13] Nevertheless, the rigid and bulky semiconductor chips have limited its uses as *in vivo* devices due to incongruent contact with the corrugated and curved surfaces of organs such as the brain, eye, and heart. Especially, artificial retina systems recently approved by the Food and Drug Administration (FDA) require extremely slim and pliable large-scale integration (LSI) for conformal settlement on the outside of the eyeball.[14,15]

Several researchers have fabricated high-performance flexible electronics after transferring micropatterned silicon nanomembranes onto plastic substrates to develop transistors, monolithic integrated circuits (ICs, tens of interconnected transistors), and biointegrated devices.[16−21] We have also reported fully functional flexible resistive

* Address correspondence to keonlee@kaist.ac.kr.

Received for review March 11, 2013 and accepted April 25, 2013.

Published online April 25, 2013
10.1021/nn401246y

random access memory (RRAM) using ultrathin single-crystalline silicon switching elements.[22] However, the realization of LSI for a future flexible mobile application process (AP) or high-density dynamic random access memory (DRAM) is still a long-term goal to be solved. The main problem with the above-mentioned approaches is that the transferred micro-sized silicon on flexible substrates has a very difficult multilayer nanoscale metal interconnection (*i.e.*, approximately eight metal layers for a state-of-the-art microprocessing unit, MPU). Moreover, the alignment inaccuracies at the nanoscale, caused by the misalignment of silicon membranes and thermal expansion of polymer substrates, aggravate the scaling down to nanotransistors on plastics.[23]

Another critical issue related to flexible biointegrated electronics is the short lifetime offered by the packaging technology.[24] Previous flexible substrates and wrapping materials such as polyimide, polydimethylsiloxane (PDMS), and parylene-C cannot monolithically encapsulate devices due to their disparate interface with each other.[25,26] Flexible packages of these polymers do not effectively prevent moisture infiltration through the discrete boundary of lamination, which causes device failure or toxic elements to be spread within the human body. Therefore, an innovative packaging technology is required to extend the lifetime of implanted flexible electronic systems which have biocompatible material issues.

Liquid crystal polymers (LCPs) have been spotlighted as a stable and long-lasting material for both flexible substrates and packaging materials in *in vivo* conditions. Our group has developed LCP-based neural signal recording microelectrodes and light-emitting diodes (LEDs) for next-generation flexible biomedical electronics.[27−30] In particular, LCP monolithic encapsulation for metal microarrays has been proven as a reliable electronic packaging of *in vivo* medical applications due to its high interfacial adhesion, biocompatibility, and extremely low degree of moisture absorption compared to other polymers.[31] LCPs also have small volume, light weight, and cost-effective advantages over conventional ceramics and titanium materials used in clinical devices, such as the artificial cardiac pacemaker and sacral nerve stimulator.[24] Notwithstanding their benefits, monolithically encapsulated LCP packaging technologies have not been exploited for flexible semiconductor ICs and their implantable biomedical applications.

Herein, we report the *in vivo* ultrathin silicon-based flexible radio frequency integrated circuits (RFICs) fabricated with 0.18 μm RF CMOS process, which are essential parts of implantable devices for wireless communication.[32] Biocompatible LCPs are used for the first time as a flexible substrate and monolithic encapsulation for high-performance flexible RFICs. Through finite element analysis (FEA) simulation, it is confirmed that the LCP-encapsulated structure is more stable than non-encapsulated IC devices in a harsh bending condition, like under movements of the human body. Finally, the LCP monoencapsulated RFICs are implanted into rats to test their stable operation under *in vivo* circumstances. An Arrhenius calculation using *in vitro* soak tests is also performed to theoretically predict the estimated lifespan of *in vivo* LCP monoencapsulated RFIC devices. The obtained results could open up a possibility to realize flexible LSI for *in vivo* biomedical applications.

RESULTS AND DISCUSSION

Figure 1a shows the fabrication schematic diagrams of LCP monoencapsulated flexible RFICs. (i) The high-performance RFICs consisting of roughly 1000 nanoscale transistors are constructed on the ultrathin top silicon layer (145 nm) of SOI wafers by 0.18 μm RF SOI CMOS process (see Supporting Information for the circuit layout of RFICs on SOI, Figure S1) with three layers of metal interconnect. (ii) After a wafer sealing process, the sacrificial bottom silicon is removed in boiling aqueous alkaline solutions of potassium hydroxide (KOH) or tetramethylammonium hydroxide (TMAH).[33] The elimination of silicon stops when the anisotropic etching solution meets the BOX layer. (iii) The flexible RFIC devices are transferred onto a LCP substrate (50 μm in thickness) coated with silicone adhesive. (iv) The flexible devices on LCP substrates are monoencapsulated with another LCP cover (25 μm in thickness) by a thermal press bonding process at a temperature of 285 °C and pressure of 2.1 MPa. The monolithic structure of LCP encapsulation blocks the penetration of ions and moisture through the LCP seals.[28] (v) Finally, the LCP monoencapsulated RFICs are implanted under the skin of a live rat (see Supporting Information for details on the fabrication of flexible RFICs on LCP substrates, Figure S2).

Figure 1b shows a conceptual schematic of an artificial retinal implant utilizing a flexible LSI wireless communication chip. The LCP monoencapsulated flexible LSI system could naturally adhere to the round surface of the eyeball. Figure 1c shows a magnified optical image of nanotransistors, passive components (capacitors and resistors), and RF switches consisting of 60 integrated nanotransistors, transferred onto a LCP substrate. Figure 1d shows completely bent flexible RFICs on a LCP substrate, and its inset represents the device on three curvilinear glass rods. In order to achieve mechanically stable device performance of the flexible nanointegrated RF switches, ultrathin active semiconductor materials would be very beneficial for high device bendability on plastic substrates.[22,34] Figure 1e shows a cross-sectional scanning electron microscopy (SEM) image of the flexible RFICs on a LCP substrate. The 6 μm thickness of the RFICs' layer bonds on silicone adhesive.

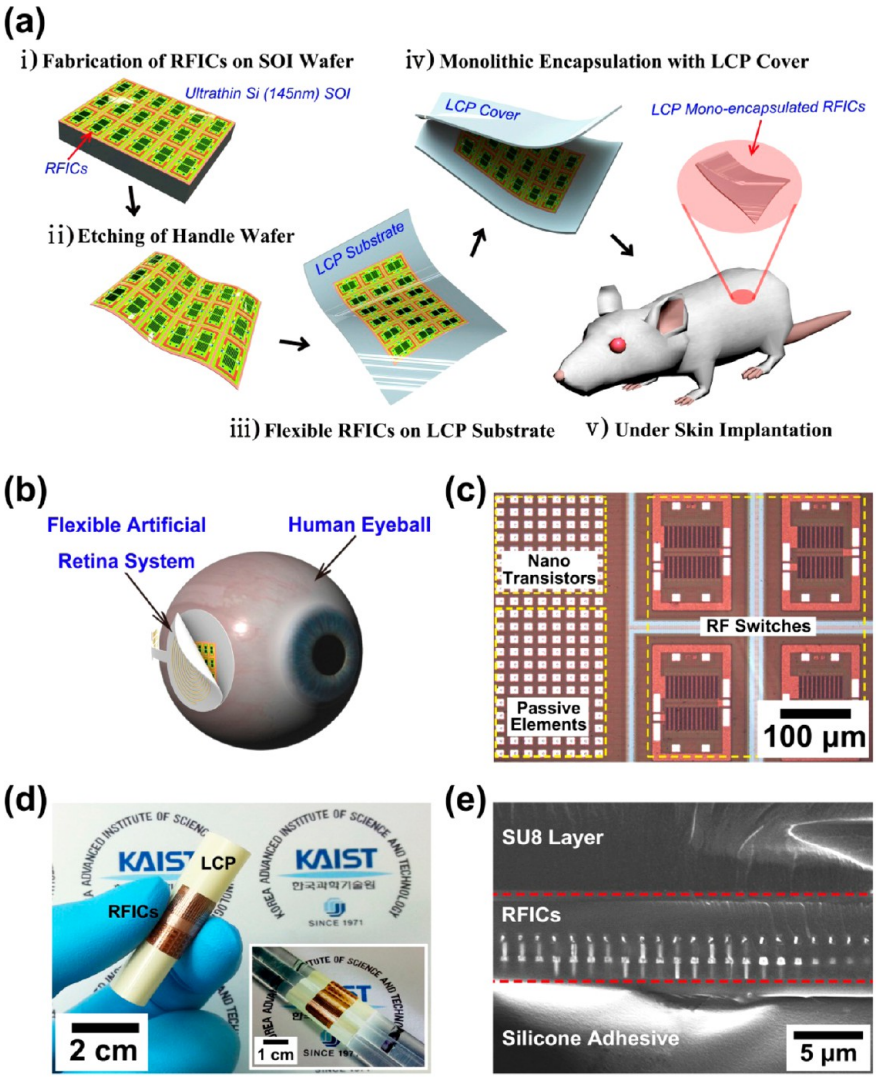

Figure 1. (a) Schematic illustration of the process for fabricating *in vivo* flexible RFICs. (b) Artistic conception of a thin and flexible subretinal implant system. (c) Optical microscopy image of RF switches and other circuit components (nanotransistors and passive elements) on a flexible substrate. (d) Photograph of flexible RFICs on a LCP substrate. The inset shows that the flexible RFICs can provide conformal contact on curvilinear surfaces of three glass pipets. (e) Cross-sectional SEM image of the flexible RFICs on a LCP substrate.

Figure 2a presents the bonding mechanism of the LCP monolithic process. LCPs are wholly aromatic polyester based on rigid and flexible monomer units. Heat and pressure lead to the glass transition of overlapped LCPs and the subsequent chemical cross-linking process of polymer chains on facing LCP surfaces, as depicted in the bottom schematic of Figure 2a. The comparison of induced stresses on RFIC silicon membranes with and without a top LCP encapsulation layer is carried out by COMSOL simulation software to calculate the improvement of fracture resistance of the LCP monoencapsulated flexible RFICs on severely curved surfaces (*e.g.*, human organs and moving tissues). Figure 2b-i shows the schematic of the four-point-bending setup for the simulation. In this case, the thicknesses of the bottom LCP substrate/adhesive/RFICs/SU-8/top LCP encapsulation are set to 50/10/6/10/25 μm, respectively. The variation of in-plane stresses for the RFICs is analyzed as a function of bending force, as shown in Figure 2b-ii. The stress in the silicon membrane with laminated LCP is smaller than that without a top LCP capping, by a factor of approximately 23. This result can be explained by the fact that the active layer of LCP monoencapsulated RFICs is placed near the mechanical neutral plane which effectively reduces in-plane stress.[35] Figure 2c is a photograph of LCP monoencapsulated flexible RFICs interposed between the skin and hypoderm of a rat. The inset of Figure 2c shows that the device is positioned under the incised epidermis. The 100 μm thickness of implanted packaging provides sufficient flexibility to fit into the curved subcutaneous layer, and the flexibility of LCP monoencapsulated RFICs can increase with thickness reduction of the LCP substrate and top LCP.[20] After suturing, the device is completely covered by rat skin, as shown in the inset of Figure 2d,

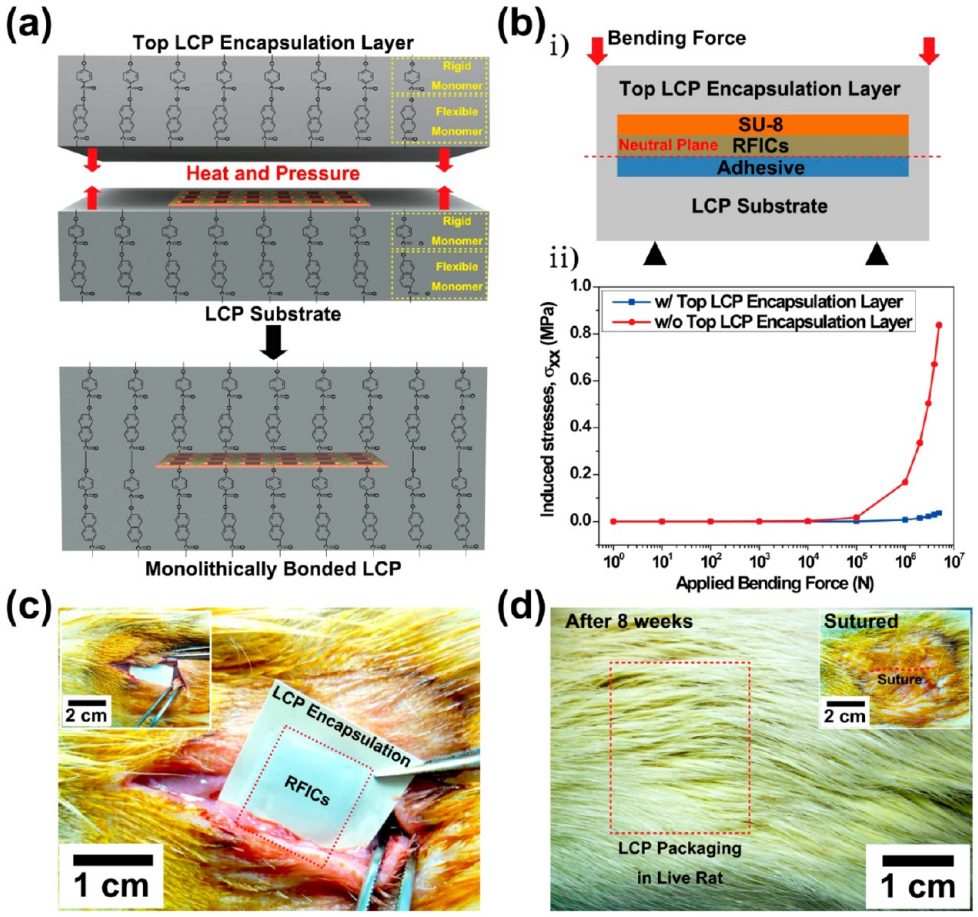

Figure 2. (a) Process schematic of chemically bonded LCP by heat and pressure monolithic process. (b) Geometry of four-point-bending test for FEA simulation (i). Calculated in-plane stresses at silicon membranes of flexible RFICs *versus* applied bending force for with/without top LCP encapsulation (ii). (c) Images of implant procedure for LCP-encapsulated device in the flank region of rat. (d) Implant site shortly after stitching up the wound (inset) and 8 weeks after. The LCP packaged flexible device is fully embedded into the subcutaneous layer of rat.

without any silhouette of implanted LCP encapsulation on the skin surface. In addition, Figure 2d shows that the wound has recovered from its original suture without liquid buildup or abscess during eight weeks observation. These *in vivo* inflammatory evaluations with our previous reports of *in vivo* implants and *in vitro* cytotoxicity assays demonstrate the bioaffinity of LCP monolithic encapsulation in a living animal.[28,31]

Figure 3a shows an optical top view of the nano-NMOSFET on flexible LCP substrates. The NMOSFETs on plastics have a channel length of 320 nm, channel width of 5 μm, and gate oxide thickness of 6 nm. The nano-MOSFETs' manufacturing process is optimized by adopting many RF CMOS technologies such as SOI halo implant, lightly doped drain, and antipunch through to minimize signal loss and short channel effects, as depicted in the inset of Figure 3a.[36,37] We believe that scaling down of flexible transistors to a few tens of nanometer scale can be achieved by further engineering efforts.

Figure 3b shows the transfer curves on bulk and flexible substrates composed of output drain current (I_D) as a function of input gate bias (V_G) at a drain voltage (V_D) value of 0.1 V in the linear regime, and the inset of Figure 3b shows logarithmic scale. Figure 3c presents the output performance (I_D-V_D curves) of NMOSFETs with sharp I_D saturation behavior on the V_D at various V_G. The switching transistors on plastics exhibit high-performance electrical properties with an effective mobility (μ_{eff}) of 400 cm^2/V·s, on/off ratio of 10^8, and threshold voltage of 0.26 V. The electrical characteristics in Figure 3b,c indicate that the values of saturated I_D and μ_{eff} decrease to ~15% after the NMOSFET transferred onto the flexible substrate. These results might be due to increased contact resistance between the probe tips and MOSFET metal pads.[38] The soft nature of the plastic substrate and the adhesion layer under the metal pads could reduce the contact force of the probe tips, which would cause variation of the contact resistance.[39] Additional process and measurement optimization would curtail the degradation of saturated I_D and μ_{eff}. The transconductance differences (g_m/g_{mo}) between bent and unbent states of NMOSFETs on plastics are plotted in Figure 3d at a surface strain of up to 0.25%, which corresponds to a bending radius of 10 mm. The mechanical stability of

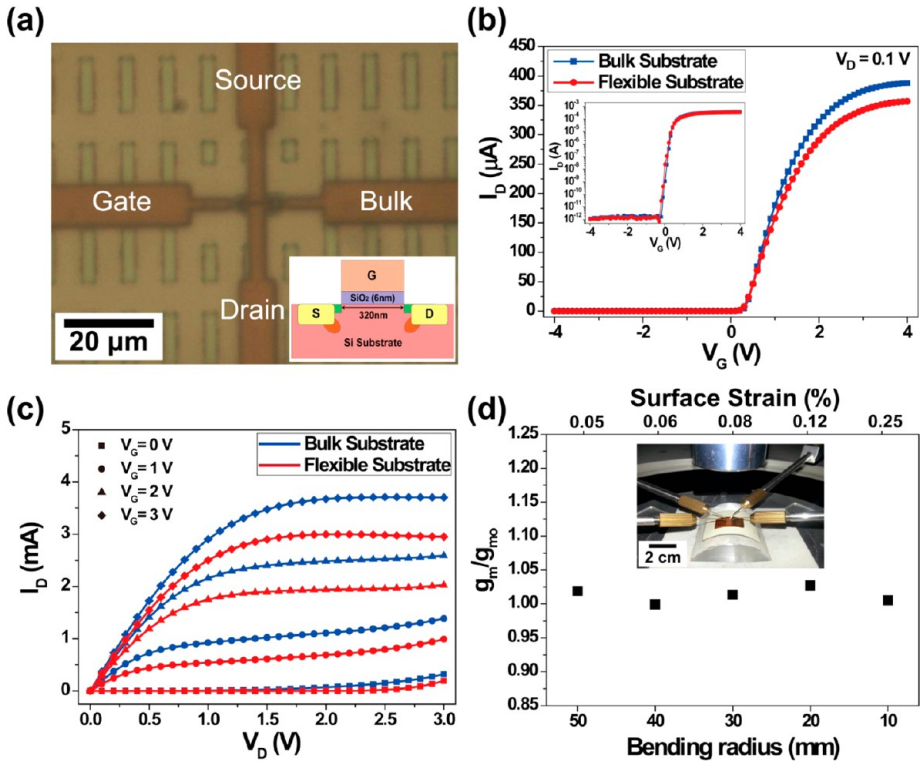

Figure 3. (a) Magnified optical image of flexible nano-NMOSFET. The inset shows schematic cross-sectional view of nano-NMOSFET with a channel length and channel width of 320 nm and 5 μm, respectively. (b) Linear and log scale (inset) plots of transfer characteristics of the flexible NMOSFET before (blue lines) and after (red lines) transfer process onto a LCP substrate. (c) Typical current−voltage curves of the flexible NMOSFET. From the bottom to top, V_G varies from 0 to 3 V. (d) Transconductance changes (g_m/g_{mo}) as a function of bending radius and surface strain. The inset is a photograph of electrical measurement being performed under a bended condition.

the flexible transistors is verified by the small changes of g_m/g_{mo} within error margin.

Figure 4a shows an optical image of flexible single-pole-single-throw (SPST) RF switches, extensively used as a gateway for wireless communication and its corresponding equivalent circuit. Direct current (DC) bias of 2.5 and 0 V is, respectively, applied on equivalent MOSFET M1 and M2 in order to turn the RF switches on, so an inputted RF signal can be transmitted to output port through M1: "on state". On the other hand, an inputted RF signal would be blocked by the closed gate of M1 by applying voltage bias of 2.5 V to M2 and 0 V to M1: "off state". The forward transmission gain (S_{21}) can be defined as the power ratio of input signal to output signal, called insertion loss at on state or isolation at off state. The return loss (S_{11}) is defined as the power ratio of input signal to reflected signal. The measured value of scattering parameter from 0.05 to 3 GHz at on state or off state for the RF switches is shown in Figure 4b,c, respectively. At on state, the RF switch has low insertion loss of less than 1 dB and return loss of ~22 dB. The switch shows superior isolation of larger than 26 dB under off state with the return loss of 3 dB, as depicted in the inset of Figure 4c. The high performance of the flexible RF switches comes from the superb electronic properties of ultrathin single-crystalline silicon nanomembranes and the well-optimized 0.18 μm RF SOI CMOS process.[21] Figure 4d presents the S_{21} values under bending fatigue tests at on and off states with repeated bending cycling corresponding to the three bending states of flexible RFIC devices, as shown in Figure 4e. The device retains its high mechanical robustness and durability over 1000 bending cycles at a curvature radius of 10 mm. The flexible RF switches at the frequency of medical implant communication service (MICS) and industrial scientific medical (ISM) band have the potential for advanced development of flexible biomedical wireless circuits.[32]

In vivo animal experiments are performed for six weeks to demonstrate the RF response stability of LCP monoencapsulated flexible RFICs in a live body. Figure 5a gives a schematic outline of the implantable and flexible RF switch connected with metal electrodes onto a SU-8 interlayer dielectric for measurement. Figure 5b shows an *in vivo* electrical measurement of the LCP monoencapsulated RFIC device inserted for six weeks in the left flank of live rat. A printed circuit board (PCB) is assembled with the external part of the electrode array, which links together a network analyzer for monitoring the frequency response properties. Figure 5c presents the S_{21} changes of the RF switch at 2.45 GHz (ISM band) inside the animal bodies during the test period. The *in vivo* insertion loss is maintained

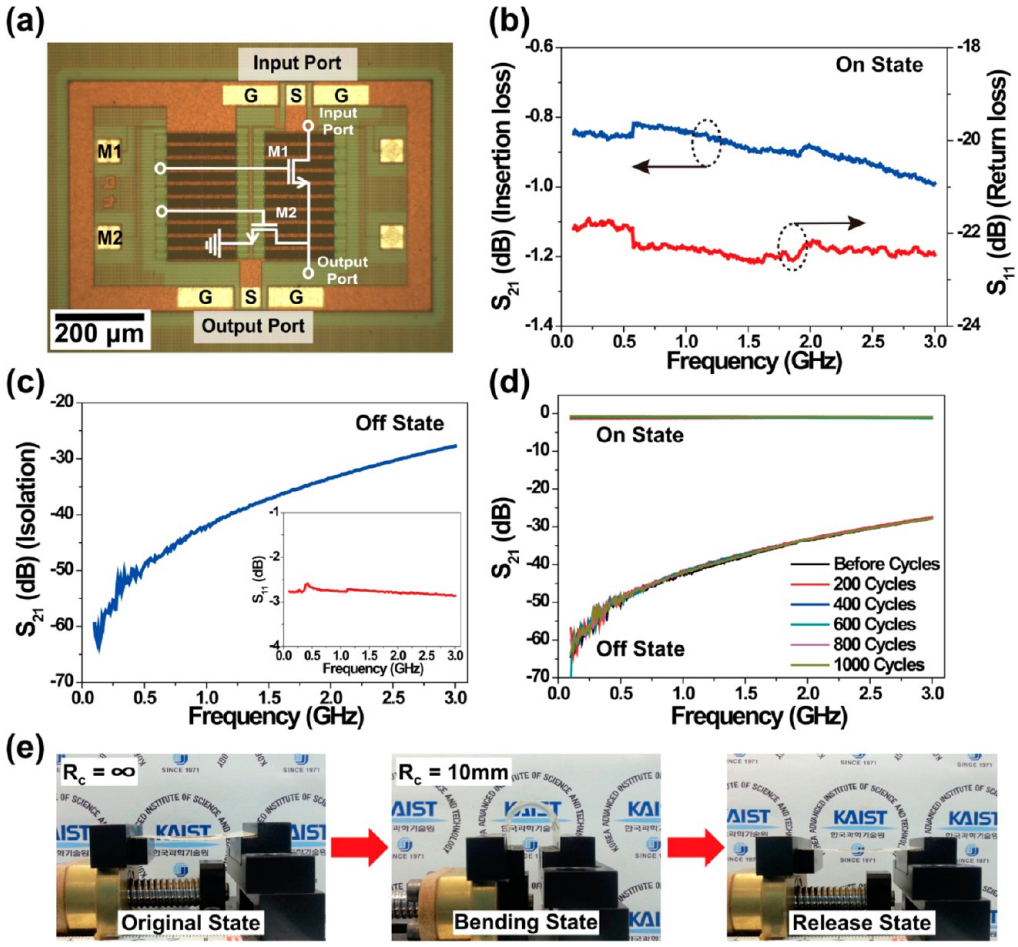

Figure 4. (a) Optical microscope image of the flexible RF switch with circuit diagram. The metal pads labeled as *G*, *S*, and V_G are for ground, signal, and gate voltage, respectively. (b) Measured S_{21} (insertion loss) and S_{11} (return loss) of RF switch at on state. (c) Measured S_{21} (isolation) and S_{11} (inset) under off state. (d) Continuous bending fatigue test results up to 1000 iterations for the RF switch under on and off states. (e) Optical images of the flexible RFICs in their original, bending, and release states for bending fatigue test.

at ~2.5 dB, while isolation is formed near 28 dB. These outstanding results indicate that the LCP monoencapsulated flexible RFICs retain constant performance under short-term *in vivo* conditions without device degradation. The basic performance of the implantable RF switches at both on and off states is slightly declined compared to the Figure 4b,c due to parasitic components caused by extended PCB connection.

To calculate the *in vivo* lifetime of LCP monoencapsulated RFICs, long-term *in vitro* accelerated soak tests are conducted with theoretical Arrhenius approach. The LCP packaged nanotransistors are soaked in phosphate-buffered saline (PBS) solutions at three different temperatures of 75, 85, and 95 °C. If PBS permeates through the bonding interface of LCP encapsulation, the transistors would be destroyed by the penetrating salty solution which induces electrical leakage current, metal line corrosion, and device deformation. The time-to-failure (t_f) is the length of duration from putting the LCP monoencapsulated transistors into PBS solutions until those devices lose their switching action. Figure 5d plots an Arrhenius curve based on the linear fitting of $\ln(t_f)$ *versus* $1000/T$ to estimate the failure time of LCP monoencapsulated transistors. An Arrhenius equation and accelerated factor (AF) between two temperatures are given as eqs 1 and 2.[40]

$$\ln\left(\frac{1}{t_f}\right) = \ln(A) - \frac{E_a}{kT} \quad (1)$$

$$\mathrm{AF} = e^{\left(\frac{E_a}{k}\right)\left(\frac{1}{T_2} - \frac{1}{T_1}\right)} = \frac{t_{f2}}{t_{f1}} \quad (2)$$

where A, E_a, k, and T are pre-exponential factor, activation energy (eV) for failure of LCP encapsulation, Boltzmann's constant, and temperature in degrees Kelvin, respectively. The activation energy is calculated to be 0.5 eV from the slope ($-E_a/k$) of the Arrhenius graph, which is dominantly determined by the interfacial bonding strength and water absorption rate of the LCP packaging.[41,42] The t_f of LCP monoencapsulated RFICs at human body temperature (37 °C) can be predicted by eq 2 by substituting two selected temperatures of PBS solution and 37 °C (details of this

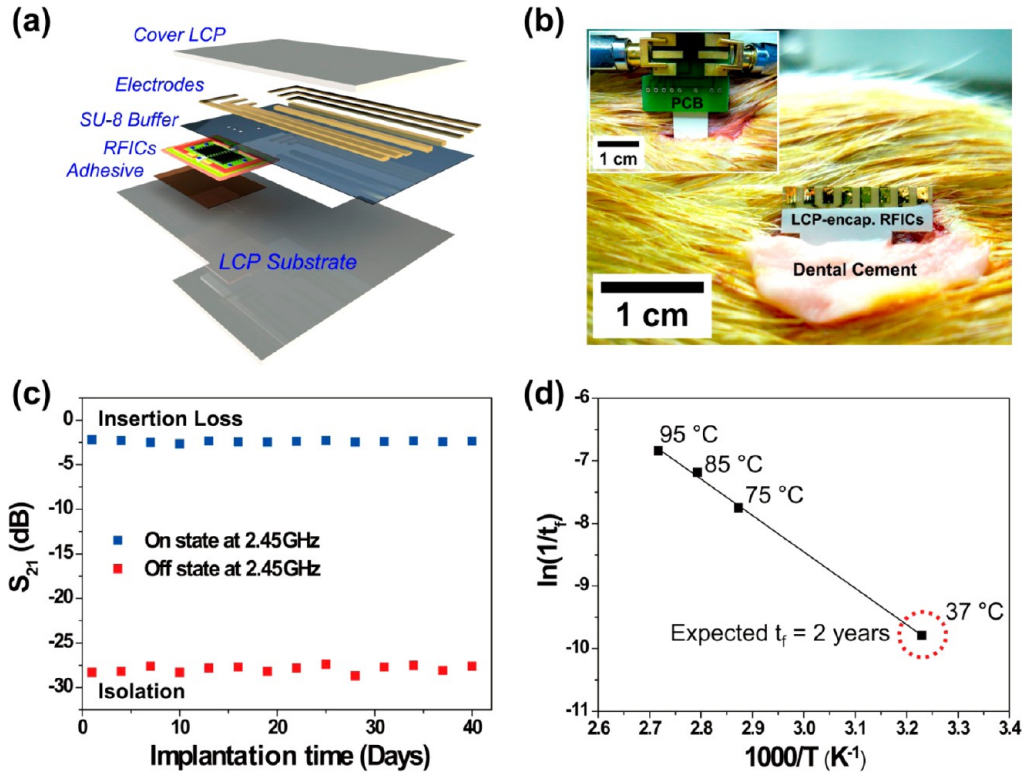

Figure 5. (a) Expanded schematic illustration of the LCP monoencapsulated RFICs. (b) Photograph of the LCP monoencapsulated flexible RFICs inserted in rat skin and connected with a PCB for *in vivo* measurement (inset). (c) Insertion loss and isolation values of *in vivo* flexible RF switch for six weeks. (d) Arrhenius plot of $\ln(1/t_f)$ *versus* $1000/T$ illustrates the temperature-dependent stability of LCP monoencapsulated devices.

process are presented in Supporting Information). From the *in vitro* accelerated soak tests and Arrhenius model, the lifespan of LCP monoencapsulated RFICs is estimated to be 2 years in a physiological environment, which is enough for preclinical applications.

CONCLUSIONS

We have fabricated high-performance LCP monoencapsulated flexible RFICs as a practical demonstration of an *in vivo* flexible LSI system. The ultrathin active layer of a silicon nanomembrane can contribute to the durable bendability of flexible RFIC devices. FEA simulation shows that the in-plane stress of flexible RFICs is reduced with our LCP monoencapsulated structure, and excellent electrical performance and mechanical stability of the devices are also proved by electrical measurements and harsh bending tests. The LCP monoencapsulated RFICs exhibit reliability and biocompatibility in *in vivo* animal experiments. Moreover, *in vitro* accelerated soak tests with the Arrhenius equation give an expected device lifetime of 2 years in a human body. These results suggest the promise of a flexible LSI, which can conform to the soft nature of curvilinear organs, for advanced biointegrated electronics such as retinal implant, BSN system, and brain–computer interface. The flexible LSI results also can be extended to realize very large-scale integration (VLSI) for consumer electronics including mobile application process (AP), high-capacity memory, and wireless communication.[22,43,44] We are currently investigating the roll-to-roll process to facilitate mass production of flexible LSI on large-area plastics (see Supporting Information for a schematic of roll-based production of flexible LSI, Figure S7).

METHODS

Flexible RFICs on LCP Substrates. The fabrication of RF switches and other circuit elements begins with 8 in. p-type (boron-doped; 10–20 Ω·cm) SOI wafers (Soitec, Unibond) by the 0.18 μm RF CMOS process. The SOI consists of a p-type ultrathin top silicon layer with (100) orientation (145 nm in thickness), a buried oxide layer (BOX, 1 μm in thickness), and a handle wafer (720 μm in thickness). Polymer adhesive (Microchem, SU-8) of 10 μm thickness is spin-coated on both unit circuit block (2 cm × 1.5 cm) on the SOI and another silicon wafer pair (650 μm in thickness) for mechanical supporting of SOI, and then bonding each other at 95 °C with applying pressure using tweezers. The wafer stack is covered by PDMS (Dow Corning, Sylgard 184) with the subsequent opening of etching window to prevent permeation of wet etchant into the bonding interface. The wet etching process with 10% KOH solution (85 °C for 6 h) and 5% TMAH (75 °C for 1 h) removes the handle wafer. Flexible RFIC layer is transferred onto a 50 μm thick LCP substrate (Kuraray, Vecstar Series) coated by a pressure-sensitive silicone adhesive (Dow Corning, 7657 Adhesive).

Residual SU-8 on the flexible RFICs is removed by acetone or oxygen plasma etching.

LCP Monolithic Encapsulation. After transferring the flexible RFIC layer on LCP substrates, SU-8 of 10 μm thickness is coated partially for the buffer layer. Chromium/gold (20/400 nm) metal electrodes are photopatterned with photoresist (Clariant, AZ5214) and then wet-etched using gold (Transene, TFA) and chromium (Transene, 905N) etchants. The flexible RFICs on a LCP substrate are monolithically bonded with a LCP cover (25 μm in thickness) by thermal press (Carver, 4386 Heated Press). A PCB is connected to the LCP encapsulation for electrical measurements.

***In Vivo* Animal Tests and *In Vitro* Soak Tests.** All animal experimentations are performed in compliance with the animal experiment ethics committee regulations of KAIST. Wistar rats are anesthetized with Zoletil 50 (Virbac), and an incision is made on the flank epidermis of live rats. The LCP monoencapsulated RFICs are implanted between skin and subcutaneous tissues. Accelerated *in vitro* soak experiments are performed in specially manufactured bottles. LCP monoencapsulated nanotransistors are soaked in PBS solutions at three accelerated conditions (75, 85, and 95 °C).

Electrical Measurements. An Anritsu 65 GHz vector network analyzer 37397D is used to characterize the RF switching properties of both flexible and *in vivo* RFICs. Electrical measurements of flexible MOSFETs are carried out using a Keithly 4200 semiconductor characterization system.

Conflict of Interest: The authors declare no competing financial interest.

Acknowledgment. This research was supported by Basic Science Research Program (CAFDC-2012-0000824, NRF-2012R1A2A1A03010415), Smart IT Convergence System of Global Frontier Project (2012M3A6A6054187) funded by the Korea government (MEST) through the National Research Foundation of Korea (NRF), Development of Manufacturing Technology for Flexible Electronics with High Performance (SC0970) funded by Korea Institute of Machinery and Materials (KIMM). We thank H.-K. Bae, J. S. Oh, and M.-H. Kang in National Nanofab Center (NNFC) for supporting 0.18 μm RF SOI CMOS-based RFIC fabrication.

Supporting Information Available: Layout of CMOS-based RFICs, fabrication schematics for flexible RFICs on the LCP substrates, durability test of flexible MOSFET, statistical characteristics of flexible MOSFETs, measured S_{21} of the flexible RF switch under different bending radiuses, lifetime prediction of LCP monoencapsulated RFICs, schematic of the roll-to-roll production of flexible LSI. This material is available free of charge *via* the Internet at http://pubs.acs.org.

REFERENCES AND NOTES

1. Levine, M.; Roberts, L.; Smith, O. If I Only Had A... *Science* **2002**, *295*, 995–995.
2. Yang, G.-Z. *Body Sensor Networks*; Springer: New York, 2006.
3. Wise, K. D.; Sodagar, A. M.; Yao, Y.; Gulari, M. N.; Perlin, G. E.; Najafi, K. Microelectrodes, Microelectronics, and Implantable Neural Microsystems. *Proc. IEEE* **2008**, *96*, 1184–1202.
4. Jeong, G. S.; Baek, D. H.; Jung, H. C.; Song, J. H.; Moon, J. H.; Hong, S. W.; Kim, I. Y.; Lee, S. H. Solderable and Electroplatable Flexible Electronic Circuit on a Porous Stretchable Elastomer. *Nat. Commun.* **2012**, *3*, 977.
5. Kim, D. H.; Viventi, J.; Amsden, J. J.; Xiao, J. L.; Vigeland, L.; Kim, Y. S.; Blanco, J. A.; Panilaitis, B.; Frechette, E. S.; Contreras, D.; *et al.* Dissolvable Films of Silk Fibroin for Ultrathin Conformal Bio-integrated Electronics. *Nat. Mater.* **2010**, *9*, 511–517.
6. Klauk, H.; Halik, M.; Zschieschang, U.; Eder, F.; Schmid, G.; Dehm, C. Pentacene Organic Transistors and Ring Oscillators on Glass and on Flexible Polymeric Substrates. *Appl. Phys. Lett.* **2003**, *82*, 4175–4177.
7. Ju, S. Y.; Facchetti, A.; Xuan, Y.; Liu, J.; Ishikawa, F.; Ye, P. D.; Zhou, C. W.; Marks, T. J.; Janes, D. B. Fabrication of Fully Transparent Nanowire Transistors for Transparent and Flexible Electronics. *Nat. Nanotechnol.* **2007**, *2*, 378–384.
8. Eda, G.; Fanchini, G.; Chhowalla, M. Large-Area Ultrathin Films of Reduced Graphene Oxide as a Transparent and Flexible Electronic Material. *Nat. Nanotechnol.* **2008**, *3*, 270–274.
9. Ishikawa, F. N.; Chang, H. K.; Ryu, K.; Chen, P. C.; Badmaev, A.; De Arco, L. G.; Shen, G. Z.; Zhou, C. W. Transparent Electronics Based on Transfer Printed Aligned Carbon Nanotubes on Rigid and Flexible Substrates. *ACS Nano* **2009**, *3*, 73–79.
10. Lu, X. M.; Xia, Y. N. Electronic Materials—Buckling down for Flexible Electronics. *Nat. Nanotechnol.* **2006**, *1*, 163–164.
11. Harrison, R. R.; Watkins, P. T.; Kier, R. J.; Lovejoy, R. O.; Black, D. J.; Greger, B.; Solzbacher, F. A Low-Power Integrated Circuit for a Wireless 100-Electrode Neural Recording System. *IEEE J. Solid-State Circ.* **2007**, *42*, 123–133.
12. Wong, L. S. Y.; Hossain, S.; Ta, A.; Edvinsson, J.; Rivas, D. H.; Naas, H. A Very Low-Power CMOS Mixed-Signal IC for Implantable Pacemaker Applications. *IEEE J. Solid-State Circ.* **2004**, *39*, 2446–2456.
13. Wise, K. D.; Anderson, D. J.; Hetke, J. F.; Kipke, D. R.; Najafi, K. Wireless Implantable Microsystems: High-Density Electronic Interfaces to the Nervous System. *Proc. IEEE* **2004**, *92*, 76–97.
14. FDA Approves First Retinal Implant for Adults with Rare Genetic Eye Disease. *U.S. Food and Drug Administration (FDA)*, http://www.fda.gov/NewsEvents/Newsroom/PressAnnouncements/ucm339824.htm (accessed Feb 25, **2013**).
15. Stieglitz, T.; Schuettler, M.; Koch, K. P. Implantable Biomedical Microsystems for Neural Prostheses. *IEEE Eng. Med. Biol.* **2005**, *24*, 58–65.
16. Menard, E.; Lee, K. J.; Khang, D. Y.; Nuzzo, R. G.; Rogers, J. A. A Printable Form of Silicon for High Performance Thin Film Transistors on Plastic Substrates. *Appl. Phys. Lett.* **2004**, *84*, 5398–5400.
17. Lee, K. J.; Motala, M. J.; Meitl, M. A.; Childs, W. R.; Menard, E.; Shim, A. K.; Rogers, J. A.; Nuzzo, R. G. Large-Area, Selective Transfer of Microstructured Silicon: A Printing-Based Approach to High-Performance Thin-Film Transistors Supported on Flexible Substrates. *Adv. Mater.* **2005**, *17*, 2332–2336.
18. Ahn, J. H.; Kim, H. S.; Lee, K. J.; Jeon, S.; Kang, S. J.; Sun, Y. G.; Nuzzo, R. G.; Rogers, J. A. Heterogeneous Three-Dimensional Electronics by Use of Printed Semiconductor Nanomaterials. *Science* **2006**, *314*, 1754–1757.
19. Kim, D. H.; Lu, N. S.; Ma, R.; Kim, Y. S.; Kim, R. H.; Wang, S. D.; Wu, J.; Won, S. M.; Tao, H.; Islam, A.; *et al.* Epidermal Electronics. *Science* **2011**, *333*, 838–843.
20. Viventi, J.; Kim, D. H.; Vigeland, L.; Frechette, E. S.; Blanco, J. A.; Kim, Y. S.; Avrin, A. E.; Tiruvadi, V. R.; Hwang, S. W.; Vanleer, A. C.; *et al.* Flexible, Foldable, Actively Multiplexed, High-Density Electrode Array for Mapping Brain Activity *in Vivo*. *Nat. Neurosci.* **2011**, *14*, 1599–1605.
21. Qin, G. X.; Yuan, H. C.; Celler, G. K.; Ma, J. G.; Ma, Z. Q. Influence of Bending Strains on Radio Frequency Characteristics of Flexible Microwave Switches Using Single-Crystal Silicon Nanomembranes on Plastic Substrate. *Appl. Phys. Lett.* **2011**, *99*, 153106.
22. Kim, S.; Jeong, H. Y.; Kim, S. K.; Choi, S. Y.; Lee, K. J. Flexible Memristive Memory Array on Plastic Substrates. *Nano Lett.* **2011**, *11*, 5438–5442.
23. Sun, L.; Qin, G. X.; Seo, J. H.; Celler, G. K.; Zhou, W. D.; Ma, Z. Q. 12-GHz Thin-Film Transistors on Transferrable Silicon Nanomembranes for High-Performance Flexible Electronics. *Small* **2010**, *6*, 2553–2557.
24. Lee, S. W.; Min, K. S.; Jeong, J.; Kim, J.; Kim, S. J. Monolithic Encapsulation of Implantable Neuroprosthetic Devices Using Liquid Crystal Polymers. *IEEE Trans. Bio-Med. Eng.* **2011**, 58.
25. Seo, J. M.; Kim, S. J.; Chung, H.; Kim, E. T.; Yu, H. G.; Yu, Y. S. Biocompatibility of Polyimide Microelectrode Array for Retinal Stimulation (Vol 24, Pg 185, 2004). *Mater. Sci. Eng., C* **2004**, *24*, 585–585.
26. Deiasi, R.; Russell, J. Aqueous Degradation of Polyimides. *J. Appl. Polym. Sci.* **1971**, *15*, 2965–2974.

27. Lee, C. J.; Oh, S. J.; Song, J. K.; Kim, S. J. Neural Signal Recording Using Microelectrode Arrays Fabricated on Liquid Crystal Polymer Material. *Mater. Sci. Eng., C* **2004**, *24*, 265–268.
28. Lee, S. W.; Seo, J. M.; Ha, S.; Kim, E. T.; Chung, H.; Kim, S. J. Development of Microelectrode Arrays for Artificial Retinal Implants Using Liquid Crystal Polymers. *Invest. Ophthalmol. Visual Sci.* **2009**, *50*, 5859–5866.
29. Lee, S. E.; Jun, S. B.; Lee, H. J.; Kim, J.; Lee, S. W.; Im, C.; Shin, H. C.; Chang, J. W.; Kim, S. J. A Flexible Depth Probe Using Liquid Crystal Polymer. *IEEE Trans. Bio-Med. Eng.* **2012**, *59*, 2085–2094.
30. Lee, S. Y.; Park, K.-I.; Huh, C.; Koo, M.; Yoo, H.; Kim, S.; Ah, C.; Sung, G.; Lee, K. Water-Resistant Flexible GaN Led on a Liquid Crystal Polymer Substrate for Implantable Biomedical Applications. *Nano Energy* **2012**, *1*, 145–151.
31. Bae, S. H.; Che, J. H.; Seo, J. M.; Jeong, J.; Kim, E. T.; Lee, S. W.; Koo, K. I.; Suaning, G. J.; Lovell, N. H.; Cho, D. I.; *et al. In Vitro* Biocompatibility of Various Polymer-Based Microelectrode Arrays for Retinal Prosthesis. *Invest. Ophthalmol. Visual Sci.* **2012**, *53*, 2653–2657.
32. Bashirullah, R. Wireless Implants. *IEEE Microw. Mag.* **2010**, *11*, S14–S23.
33. Park, K.-I.; Xu, S.; Liu, Y.; Hwang, G.-T.; Kang, S. J. L.; Wang, Z. L.; Lee, K. J. Piezoelectric $BaTiO_3$ Thin Film Nanogenerator on Plastic Substrates. *Nano Lett.* **2010**, *10*, 4939–4943.
34. Kim, D. H.; Lu, N. S.; Ghaffari, R.; Rogers, J. A. Inorganic Semiconductor Nanomaterials for Flexible and Stretchable Bio-integrated Electronics. *NPG Asia Mater.* **2012**, *4*, e15.
35. Koo, M.; Park, K.-I.; Lee, S. H.; Suh, M.; Jeon, D. Y.; Choi, J. W.; Kang, K.; Lee, K. J. Bendable Inorganic Thin-Film Battery for Fully Flexible Electronic Systems. *Nano Lett.* **2012**, *12*, 4810–4816.
36. Kuo, J. B.; Lin, S.-C. *Low-Voltage SOI CMOS VLSI Devices and Circuits*; Wiley: New York, 2001.
37. Colinge, J. P. Fully-Depleted SOI CMOS for Analog Applications. *IEEE Trans. Electron Devices* **1998**, *45*, 1010–1016.
38. Streetman, B. G.; Banerjee, S. *Solid State Electronic Devices*, 6th ed.; Pearson/Prentice Hall: Upper Saddle River, N.J., 2006.
39. Pinnel, M. R.; Bradford, K. F. Influence of Some Geometric Factors on Contact Resistance Probe Measurements. *IEEE Trans. Compon., Hybr.* **1980**, *3*, 159–165.
40. Celina, M.; Gillen, K. T.; Assink, R. A. Accelerated Aging and Lifetime Prediction: Review of Non-Arrhenius Behaviour Due to Two Competing Processes. *Polym. Degrad. Stab.* **2005**, *90*, 395–404.
41. Edell, D. Insulating Biomaterials N01-Ns-9-2323, First Quarter Progress Report October-December. *National Institutes of Health* **2002**.
42. Meeker, W. Q.; Escobar, L. A. A Review of Recent Research and Current Issues in Accelerated Testing. *Int. Stat. Rev.* **1993**, *61*, 147–168.
43. Zhai, Y. J.; Mathew, L.; Rao, R.; Xu, D. W.; Banerjee, S. K. High-Performance Flexible Thin-Film Transistors Exfoliated from Bulk Wafer. *Nano Lett.* **2012**, *12*, 5609–5615.
44. Shahrjerdi, D.; Bedell, S. W. Extremely Flexible Nanoscale Ultrathin Body Silicon Integrated Circuits on Plastic. *Nano Lett.* **2013**, *13*, 315–320.